Materials Science-Poland, 32(3), 2014, pp. 430-435
http://www.materialsscience.pwr.wroc.pl/
DOI: 10.2478/s13536-014-0222-0

VERSITA

Investigation on structure of $BaTi_{1-x}Nb_xO_3$ compound prepared by rotary-hydrothermal synthesis methods

ARSIA KHANFEKR*, MORTEZA TAMIZIFAR, RAHIM NAGHIZADEH

Department of Metallurgical and Materials Engineering, Iran University of Science and Technology (IUST), Narmak, Tehran, Iran

$BaTi_{1-x}Nb_xO_3$ compounds (with x = 0.0, 0.01, 0.03, 0.06, and 0.09) were synthesized by rotary-hydrothermal (RH) method. The process was conducted at 180 °C for 5 hours in a Teflon vessel that was rotated at a speed of 160 rpm during the hydrothermal reaction. The effects of donor concentration on the structure and properties of $BaTi_{1-x}Nb_xO_3$ compounds were investigated. The experiments for the $BaTiO_3$±Nb_2O_3 system produced by a solid state reaction at high temperature at different concentrations of niobium, with the use of RH processing have not been reported in previous works. For the phase evolution studies, X-ray diffraction patterns (XRD) were analyzed and Raman spectroscopy measurements were performed. The transmission electron microscope (TEM) and the field emission scanning electron microscope (FE-SEM) images were taken for the detailed analysis of the grain size, surface and morphology of the compound.

Keywords: *Nb-doping; chemical synthesis; microwave-hydrothermal synthesis; microstructure; perovskites*

© Wroclaw University of Technology.

1. Introduction

Barium titanate is one of the most important ferroelectric materials used in electronics ceramic industry. Development of high efficiency dielectric materials has helped to design and fabricate numerous novel devices for various applications. Among these materials both lead zirconate titanate (PZT) and barium titanate (BT) have excellent dielectric properties [1–3].

In the cubic high temperature phase, barium titanate does not show any spontaneous polarization and, hence, the system is paraelectric. Upon cooling below the Curie temperature (Tc < 120 °C), a phase transition occurs, during which positive and negative metal ions displace with respect to each other, leading to a tetragonal deformation. Due to the asymmetry in the unit cell caused by the displacement, a spontaneous polarization in the direction of the axis of tetragon appears. From the crystal chemical perspective, this series of phase transitions can be viewed as a consequence of the Ti^{+4} ions being somewhat too small to occupy the interstice created by the Ba–O framework [4, 5]. Numerous studies on developing synthesis methods for purer and finer $BaTiO_3$ powders have been reported in the literature. The hydrothermal method, unique low-temperature process, has been successful in the preparation of high-purity homogeneous and ultrafine powder of $BaTiO_3$ under environmentally friendly conditions. Compared to the traditional solid-state reaction and other wet-chemical routes (including sol-gel processing, oxalate route, and homogeneous precipitation), the hydrothermal method is low-cost and convenient to prepare $BaTiO_3$ nanoparticles without a following high temperature calcination process [4–9]. In the preceding papers on solid state methods, the results of studies with respect to processing of Nb-doped $BaTiO_3$ were reported. Specifically, it was shown that the Nb ions may be incorporated into the BaTiO3 lattice in a narrow temperature range of 1523 to 1733 K. It was also shown that at temperatures lower than 1500 K, Nb cannot be incorporated into the $BaTiO_3$ lattice due to kinetic reasons [12, 13]. Though many efforts have been devoted to prepare $BaTiO_3$ particles, there is still little

*E-mail: khanfekr@iust.ac.ir

knowledge about the effects of doping and solvent on the size and shape of this compound under hydrothermal conditions. A number of authors have synthesized $BaTiO_3$ by a microwave hydrothermal (MH) method below 200 °C but RH processing of Nb doped $BaTiO_3$ has not been reported yet. In this work we investigated the effect of niobium incorporation on the properties of $BaTiO_3$ doped with different concentration of Nb using a new microwave hydrothermal method instead of previously used high-temperature solid state reaction for the system $BaTiO_3 \pm Nb_2O_3$.

2. Experimental

The RH reactions were performed using a laboratory-made rotary-heating-autoclave system having a PTFE inner vessel with a temperature control up to 220 °C. An auxiliary cooling/heating device was fitted to the system that enabled it to operate at a fixed temperature for a long time. $BaTi_{1-x}Nb_xO_3$ compounds (with x = 0.00, 0.01, 0.03, 0.06, and 0.09) were synthesized by rotary-hydrothermal (RH) method. Reagents of $C_{16}H_{36}O_4Ti$, $Ba(OH)_2{\cdot}8H_2O$, $NbCl_5$ and NaOH were used as raw materials. The starting materials of $Ba(OH)_2{\cdot}8H_2O$, $NbCl_5$ and $C_{16}H_{36}O_4Ti$ were mixed at 70 °C in distilled water containing 1M NaOH to control the pH under stirring, until it turned into a homogeneous solution. The solution was transferred into a sealed PTFE autoclave followed by filling with distilled water until the total volume reached to 100 ml, 80 % of the capacity of the autoclave.

The system was heat treated at 180 °C for 5 h. The resulting powders were centrifuged and washed with distilled water, and finally oven dried at 85 °C for 24 h. The obtained powders were characterized by X-ray powder diffraction (XRD) (X'Pert PRO MPD) with Cu-Kα radiation in the 2θ range of 20° to 90°. Raman spectroscopy (BRUKER/ Spectral Range 80 – 3500 cm^{-1}) Microstructural characterization was performed by the field emission scanning electron microscopy (FE-SEM/MIRAII TESCAN) and transmission electron microscopy (TEM, PHILIPS-EM-208).

3. Results and discussion

Fig. 1 shows the X-ray powder diffraction patterns of the microwave-hydrothermal niobium doped barium titanate ($BaTi_{1-x}Nb_xO_3$) powders prepared at 180 °C for 5 h. The nanoparticles are pure perovskite Nb–$BaTiO_3$ without any intermediate carbonate phase that usually is observed in the 2θ equal to 24° or 42° in the solid state method [14]. The presence of $BaCO_3$ can be ascribed either to incomplete reaction or to the presence of carbonate in Ba alkali source, or to the reaction of CO_2 in air. The Nb–$BaTiO_3$ sample, crystallized by RH method in a shorter time and lower temperature, is carbonate free indicating that the microwave hydrothermal technique was successful to produce the pure crystalline nanoparticles [15].

The final tetragonal peak splitting of the reflections cannot be resolved due to overlapping of the (0 0 2) and (2 0 0) planes. However, XRD-peaks of the nanoparticles are wider than micro-size particles, thus the cubic structure cannot be totally excluded that often makes this splitting difficult to determine [10, 16].

It is clearly seen that with the enhancement of niobium for x = 0.01 and 0.03, the maximum of the peak shifts towards lower 2θ values and intensity of the peaks increases. On the other hand, for x = 0.06 and 0.09 the intensity decreases and maximum of the peak shifts towards higher 2θ values again. The result for the initial substitution is in a good agreement with the changes in the tetragonality. For the lower Nb content it has been deduced that Nb^{5+} could substitute Ti^{4+} in $BaTiO_3$ lattice because the small ionic radius of Nb^{5+} (0.064 nm) is close to that of Ti^{4+} (0.061 nm). It was reported that the substitution of Nb^{5+} for Ti^{4+} decreased the tetragonality of $BaTiO_3$ ceramics [7, 17]. On the other hand, the solubility of the dopant ions in $BaTiO_3$ lattice is limited due to the differences of radius and electrovalence between foreign ions and Ba^{2+} or Ti^{4+}. It seems that the difference between the pure and Nb added compounds results from the presence of Nb_2O_5-second phase that is observed at 2θ equal to 24° and the solubility limit is between x = 0.06 and 0.09. As a result, when in this experiment Nb content in the powder was increased

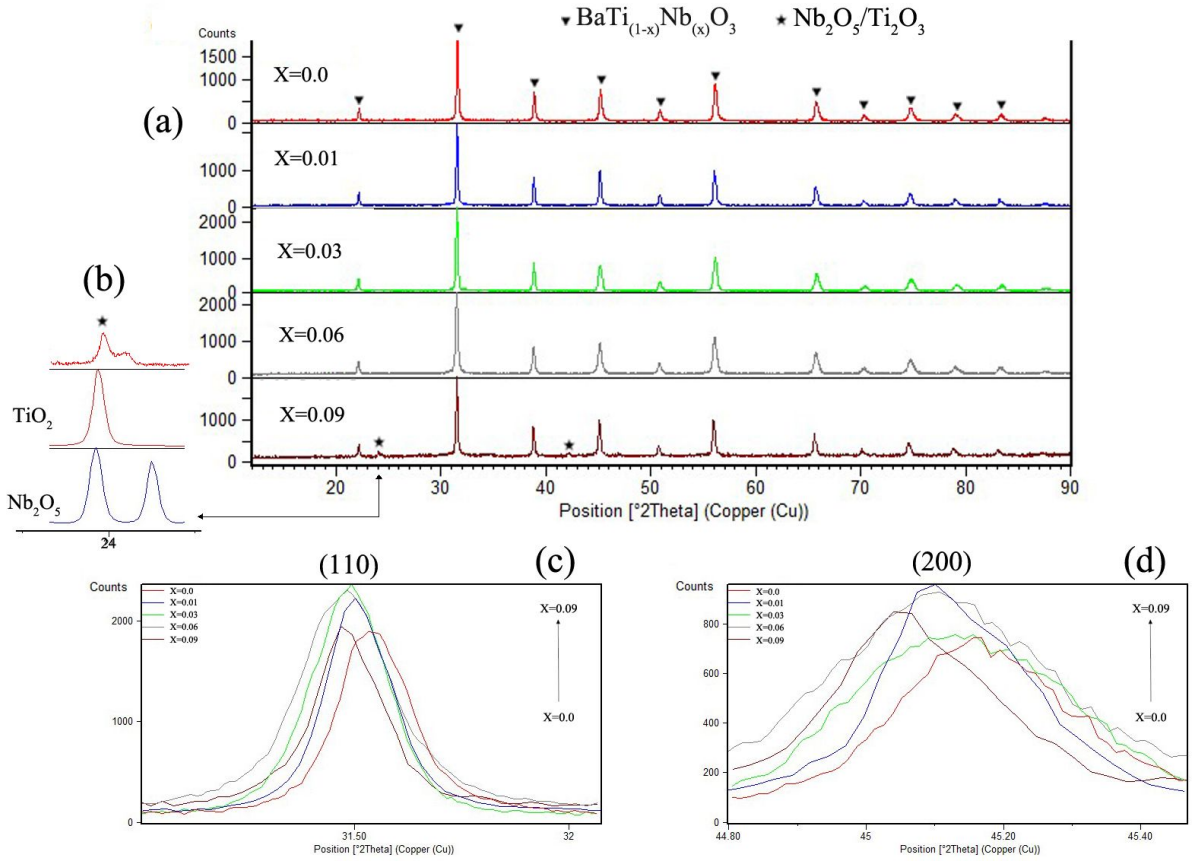

Fig. 1. (a) X-ray diffraction pattern of $BaTi_{1-x}Nb_xO_3$ nanoparticles with different compositions, and the magnified XRD patterns (b) at $2\theta = 24°$, (c) (110) planes, (d) (200) planes.

up to 0.06, some part of the powder turned out to be TiO_2 or Nb_2O_5-second phase if the Nb-source fraction was larger than the solubility limit. The secondary phase formation was due to the substitution of Nb^{5+} to Ti^{4+} site and segregation of Ti^{4+} out of $BaTiO_3$.

In order to investigate and relate these factors, the William-Hall and Scherrer methods were applied. The crystallite size of the powder was calculated using the Scherrer equation [15]:

$$D_v = \frac{K\lambda}{B_{size}\cos\theta} \tag{1}$$

where D_v is a crystallite size, K is a constant, whose value is 0.9, λ is the X-ray wavelength, and the width of the peak – B_{size} – is determined as the full width at half-maximum (FWHM). The resulted internal strain ε was calculated using the Williamson-Hall equation [18–21]:

$$B_{size+strain}\cos\theta = \frac{K\lambda}{D_v\cos\theta} + 4\varepsilon\sin\theta \tag{2}$$

For the samples of $BaTi_{1-x}Nb_xO_3$ compound (with x = 0.0, 0.03, 0.06), Fig. 2 shows the graph of $B_{size+strain}\cos\theta$ against $4\sin\theta$, plotted from equation 2, and the internal strain can be obtained from the slope of the graph. Table 1 gives the results of the calculations of internal strain and an average size of crystallites, estimated from the broadening of diffraction peak using Scherrer and Williamson-Hall equations.

According to the results, the optimization of crystal geometry of $BaTiO_3$ in tetragonal phase after doping with Nb is attained by the impurity-outward displacement of barium. Tetragonal crystal lattice results from stretching a cubic lattice along one of its lattice vectors, so that the cube

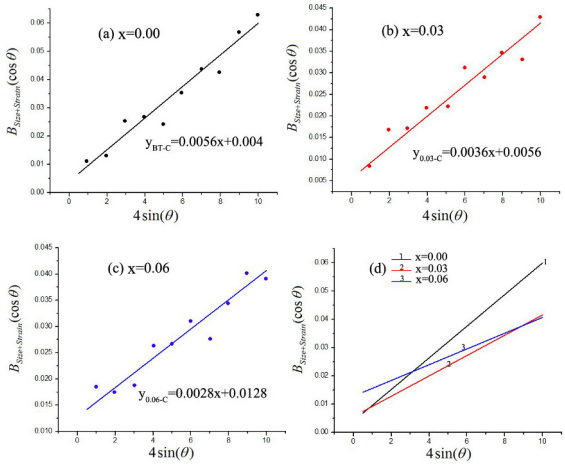

Fig. 2. Plot of $B_{size+strain}\cos\theta$ vs. $4\sin\theta$ for (a) x = 0.00; (b) x = 0.03; (c) x = 0.06; (d) all-encompassing graph.

becomes a rectangular prism with a square base (a × a) and the height (c), which is different from (a). The movements are mainly in the (a-a) plane, while the motion along the (c) axis is practically negligible. The ratio of a/c decreases with Nb concentration and finally the transition of $BaTiO_3$ crystal phase from tetragonal to cubic occurs. Therefore substitution of Nb^{5+} with bigger ionic radius for Ti^{4+} decreases the tetragonality but increases the crystallite size and internal strain.

On the other hand, based on Raman studies, the particles are tetragonal rather than cubic due to the occurrence of asymmetry of TiO_6 octahedra. The Raman spectra for the obtained Nb–$BaTiO_3$ ceramic powder samples are presented in Fig. 3. The peaks at 185 and 518 cm^{-1} are assigned to the TO mode of A1 symmetry and the sharp peak at 305 cm^{-1} is attributed to the B1 mode, which is characteristic of tetragonal $BaTiO_3$. The weak peak at 715 cm^{-1}, assigned to the highest-frequency longitudinal optical mode (LO) with A1 symmetry, is characteristic of tetragonal $BaTiO_3$ too. The peaks at 960 and 1420 cm^{-1} are assigned to Nb_2O_5 and TiO_2 or some intermediate phases like $Ti_2Nb_{10}O_{29}$ compounds [22–24]. The segregation-induced enrichment of Nb in Nb-doped $BaTiO_3$ may result in the formation of Nb-rich intergranular precipitates if the Nb concencentration is close to the solubility limit. The tetragonal fraction was calculated by measuring the intensity of the peak at 305 cm^{-1}. The intensity ratios decrease when Nb is added into the $BaTiO_3$ crystal from x = 0.01 to 0.06, and then they increase again. Niobium at lower concentrations decreases tetragonality, while close to, or above the limit of dopant solubility in barium titanate it enhances tetragonality and inhibits the powder growth.

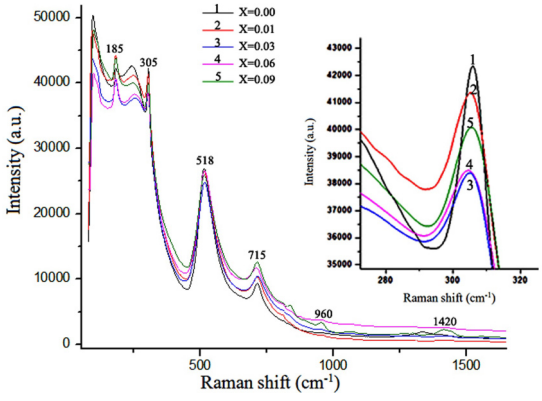

Fig. 3. Raman spectra of the hydrothermal nano-sized $BaTi_{1-x}Nb_xO_3$ powders.

The field emission scanning electron microscopy (FE-SEM) images of the prepared $BaTi_{1-x}Nb_xO_3$ compounds (with x = 0.03, 0.06) are shown in Fig. 4 and Fig. 5, respectively. The FE-SEM micrographs reveal a spherical morphology of the synthesized powders. The size of the particles is between 80 and 120 nm. In general, the microstructure obtained by the solid state method is not uniform and consists of a region of big particles, of the size more than 5 – 6 μm, and a region with fine structures of the size less than 1 – 2 μm.

The transmission electron microscope (TEM) image (Fig. 6) was taken in order to estimate the size of the grains. It also shows the morphology of the sample grains. Most particles are spherically shaped crystals with an average size of 80 nm and this result is in a good agreement with the XRD and SEM. The decreased size of the crystals obtained by the RH method might be related to the increased nucleation rate and the high mechanical energy, which activated chemical reactions at low temperatures.

Table 1. Crystallite size (nm) and microstrain (ε) of the powder, calculated by the Scherrer and Williamson-Hall equations.

x = 0.06	x = 0.03	x = 0.00	Sample
62.21	45.12	35.02	crystallite size (nm) – Scherrer
55.03	42.77	27.50	crystallite size (nm) – Williamson-Hall
0.0032	0.0014	0.0010	microstrain (ε) – Williamson-Hall

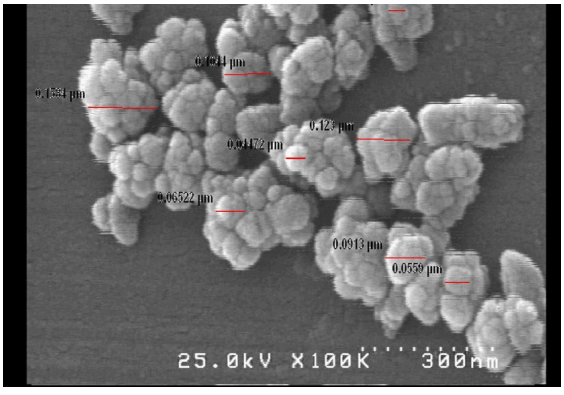

Fig. 4. $BaTi_{1-x}Nb_xO_3$ (x = 0.03) powders prepared at 180 °C for 5 h.

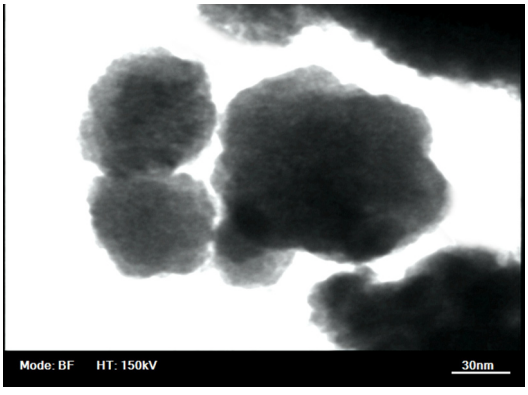

Fig. 6. TEM image of the Nb–$BaTiO_3$ powders.

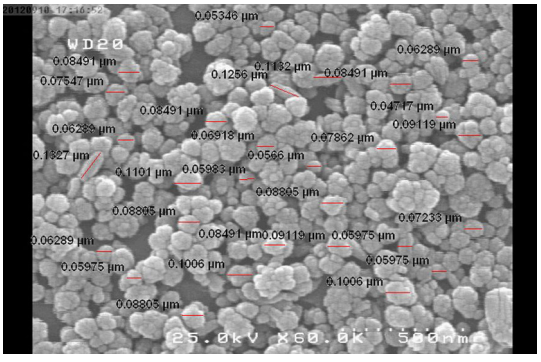

Fig. 5. $BaTi_{1-x}Nb_xO_3$ (x = 0.06) powders prepared at 180 °C for 5 h.

4. Conclusions

The present investigation shows that nanoparticle-sized Nb–$BaTiO_3$ powders can be crystallized using a rapid and cost-effective rotary hydrothermal method. Synthesis by rotary-hydrothermal method has the advantages of faster crystallization, decreased crystal size, more homogenous distribution of dopants and processing at lower temperature and shorter time in comparison with solid state methods.

The nanoparticles were pure perovskite Nb–$BaTiO_3$ without any intermediate carbonate phases that usually are observed in the solid state method. For the samples of $BaTi_{1-x}Nb_xO_3$ compound with x = 0.0, 0.03 and 0.06 it was deduced that Nb^{5+} could substitute Ti^{4+} in $BaTiO_3$ lattice and the substitution of Nb^{5+} with Ti^{4+}, characterized by a larger ionic radius, resulted in decreased tetragonality but increased crystallite size and internal strain. The solubility limit of Nb was a little less than x = 0.09 (i.e. between x = 0.06 and 0.09). Moreover, the incorporation of abundant niobium substituting the titanium site in the $BaTiO_3$ lattice produced titanium segregation or resulted in the formation of Nb-rich intergranular precipitates if Nb concentration was close to the solubility limit.

References

[1] KIM H.T., HAN Y.H., *Ceram. Int.*, 30 (2004), 1719.
[2] BOMLAI P., *Songklanakarin J. Sci. Technol.*, 28 (3) (2006), 669.
[3] YOO H.-I., SONG C.-R., *J. Electroceram.*, 6 (1) (2001), 61.

[4] CHEN C., WEI Y., JIAO X., CHEN D., *Mater. Chem. Phys.*, 110 (2008), 186.
[5] YING K.-L., HSIEH T.-E., *Mater. Sci. Eng. B-Adv.*, 138 (2007), 241.
[6] YUAN Y., ZHANG S.R., ZHOU X.H., TANG B., *J. Mater. Sci.*, 44 (2009), 3751.
[7] LIU L., GUO H., LÜ H., DAI S., CHENG B., CHEN Z., *J. Appl. Phys.*, 97 (2005), 054102.
[8] BRZOZOWSKI E., CASTRO M.S., FOSCHINI C.R., STOJANOVIC B., *Ceram. Int.*, 28 (2002), 773.
[9] SHAO Y., MAUNDERS C., ROSSOUW D., KOLODIAZHNYI T., ABOTTON G., *Ultramicroscopy*, 110 (2010), 1014.
[10] NOH H.-J., LEE S.-G., *Trans. Electr. Electron. Mater.*, 10 (2) (2009), 49.
[11] HOTTA Y., TSUNEKAWA K., ISOBE T., SATO K., WATARI K., *Mat. Sci. Eng. A-Struct.*, 475 (2008),12.
[12] NOWOTNY J., RAKAS M., *Ceram. Int.*, 20 (1994), 265.
[13] BRZOZOWSKI E., CASTRO M.S., *J. Mater. Process. Tech.*, 168 (2005), 464.
[14] BRZOZOWSKI E., CASTRO M.S., FOSCHINI C.R., STOJANOVIC B., *Ceram. Int.*, 28 (2002), 773.
[15] NEWALKAR B.L., KOMARNENI S., KATSUKI H., *Mater. Res. Bull.*, 36 (2001), 2347.
[16] CHEN C., WEI Y., JIAO X., CHEN D., *Mater. Chem. Phys.*, 110 (2008), 186.
[17] SZYMCZAK L., UJMA Z., ADAMCZYK M., PAWEŁCZYK M., *Ceram. Int.*, 34 (2008), 1993.
[18] MOTE V.D., PURUSHOTHAM Y., DOLE B.N., *J. Theor. Appl. Phys.*, 6 (2012), 6.
[19] PURUSHOTHAM E., KRISHNA N.G., *B. Mater. Sci.*, 36 (6) (2013), 973.
[20] HERRMANN M., ENGEL W., GIIBEL H., *JCPDS*, 45 (2002), 212.
[21] MEIER M., *Measuring Crystallite Size Using X-ray Diffraction, The Williamson-Hall Technique* (Draft), Department of Chemical Engineering and Materials Science, University of California, Davis, US 2005.
[22] ÁVILA H.A., RAMAJO L.A., REBOREDO M.M., CASTRO M.S., PARRA R., *Ceram. Int.*, 37 (7) (2011), 2383.
[23] MIN B., MOON S.-M., CHO N.-H., *Curr. Appl. Phys.*, 11 (3) (2011), S193.
[24] LAZAREVIĆ Z., ROMČEVIĆ N., VIJATOVIĆ M., PAUNOVIĆ N., ROMČEVIĆ M., STOJANOVIĆ B., DOHČEVIĆ-MITROVIĆ Z., *Acta Phys. Pol. A*, 115 (4) (2009), 808.

Received 2014-05-27
Accepted 2014-06-13